# $^{17}O$ and $^{27}Al$ MAS and 3QMAS NMR Study of Synthetic and Natural Layer Silicates

Sung Keun Lee[†,‡] and Jonathan F. Stebbins[†]

*Department of Geological and Environmental Sciences, Stanford University, Stanford, California 94305, and Geophysical Laboratory, Carnegie Institution of Washington, 5251 Broad Branch Road, Washington, D.C. 20015*

Charles A. Weiss, Jr.[§,||] and R. James Kirkpatrick[||]

*U.S. Army Corps of Engineers Research & Development Center, 3909 Halls Ferry Road, Vicksburg, Mississippi 39180, and Department of Geology, University of Illinois at Urbana-Champaign, 245 Natural History Building, 1301 West Green Street, Urbana, Illinois 61801*

*Received January 27, 2003. Revised Manuscript Received April 2, 2003*

We report $^{17}O$ and $^{27}Al$ NMR results for $^{17}O$-enriched synthetic and natural layer silicates with significantly improved resolution of oxygen sites including basal and apical oxygens using $^{17}O$ 3QMAS NMR spectroscopy. These oxygen sites have well-defined ranges of $^{17}O$ isotropic chemical shifts ($\delta_{iso}$) and quadrupolar coupling constants ($C_q$). The $C_q$ of basal oxygen ($^{[4]}Si-O-^{[4]}Si$) range from 4.1 to 5.2 MHz for these phases, and $\delta_{iso}$ varies from 39 to 55 ppm. The $\delta_{iso}$ value of the basal oxygen sites increases with increasing $C_q$. The $C_q$ and $\delta_{iso}$ values of apical oxygens ($^{[4]}Si-O-2^{[6]}Al$) are about 3.4 MHz and about 64 ppm, respectively, and are similar among the phases examined. The hydroxyl group ($2^{[6]}Al-OH$) has the largest $C_q$ (about 7 MHz) among the oxygen sites, as well as the most shielded chemical shift of about 37−44 ppm. Analysis of the $^{27}Al$ MAS NMR spinning sideband manifolds yields precise NMR parameters for the $^{[6]}Al$ sites. $^{27}Al$ MAS and 3QMAS NMR spectroscopies at 14.1 T yield excellent quantification of the $^{[6]}Al/^{[4]}Al$ ratio of 2 for natural muscovite. The methods described here, in particular $^{17}O$ 3QMAS at high $H_0$ field (14.1 T), are effective probes of crystallographically distinct sites with similar $C_q$ and $\delta_{iso}$ value in layer silicates and are thus potentially useful for characterizing the complex and heterogeneous natural layer silicates and other nanoscale earth materials, such as crystalline and amorphous oxyhydoxides and oxides.

## Introduction

The surfaces of layer silicates, such as micas and clay minerals, can greatly affect the chemistry of groundwater and the adsorption and transport of nuclear waste and heavy metals.[1−3] Many layer silicates, especially those formed in low-temperature environments, can be regarded as natural nano-geomaterials.[4] Layer silicates also have important applications as industrial catalysts, and there has been extensive theoretical and experimental study of their structures, stability, and reactivity.[5] The composition and distribution of cations among tetrahedral and octahedral sites often determine the surface charge, the bonding behavior of reactive sites on the grain edges, and key structural characteristics (e.g., bond angle variation),[2,6] and thus, they significantly affect many properties, including reactivity with aqueous solutions and metal adsorbates. Such detailed structural information is difficult to obtain from conventional X-ray diffraction methods, and solid-state $^{29}Si$ and $^{27}Al$ NMR spectroscopies have been important tools in exploring the short-range order and structural configuration in layer silicates.[5,7−14] Such studies have

* To whom correspondence should be addressed. Address: Geophysical Laboratory, Carnegie Institution of Washington, 5251 Broad Branch Rd. Washington, DC 20015. E-mail: s.lee@gl.ciw.edu. Phone: 202-478-8968. Fax: 202-478-8901.

† Stanford University.

‡ Carnegie Institution of Washington.

§ U.S. Army Corps of Engineers Research & Development Center.

|| University of Illinois at Urbana-Champaign.

(1) Brown, G. E.; Henrich, V. E.; Casey, W. H.; Clark, D. L.; Eggleston, C.; Felmy, A.; Goodman, D. W.; Gratzel, M.; Maciel, G.; McCarthy, M. I.; Nealson, K. H.; Sverjensky, D. A.; Toney, M. F.; Zachara, J. M. *Chem. Rev.* **1999**, *99*, 77−174.

(2) Sposito, G.; Skipper, N. T.; Sutton, R.; Park, S. H.; Soper, A. K.; Greathouse, J. A. *Proc. Natl. Acad. Sci. USA.* **1999**, *96*, 3358−3364.

(3) Kim, Y.; Kirkpatrick, R. J.; Cygan, R. T. *Geochim. Cosmochim. Acta* **1996**, *60*, 4059−4074.

(4) Navrotsky, A. In *Nanoparticles and the Environment*; Banfield, J. F., Navrotsky, A., Eds.; Mineralogical Society of America: Washington, DC, 2001; Vol. 44.

(5) Haddix, G. W.; Narayana, M. In *NMR Techniques in Catalysis*; Bell, A. T., Pines, A., Eds.; Marcel Dekker: New York, 1994; p 432.

(6) Lasaga, A. C. In *Chemical Weathering Rates of Silicate Minerals*; White, A. F., Brantley, S. L., Eds.; Mineralogical Society of America: Washington, DC, 1995; Vol. 31, pp 23−86.

(7) Altaner, S. P.; Weiss, C. A.; Kirkpatrick, R. J. *Nature* **1987**, *331*, 699−702.

(8) Herrearo, C. P.; Gregorkiewitz, M.; Sanz, J.; Serratosa, J. M. *Phys. Chem. Miner.* **1987**, *15*, 84−90.

(9) Kirkpatrick, R. J. In *Spectroscopic Methods in Mineralogy and Geology*; Hawthorne, F. C., Ed.; Mineralogical Society of America: Washington, DC, 1988; pp 341−403.

(10) Thompson, A. R.; Botto, R. E. *Energy Fuels* **2001**, *16*, 257−271.

10.1021/cm030165h CCC: $25.00 
Published on Web 05/24/2003

provided important insight into such structural details as the tetrahedral Si/Al distribution, the distribution of Al on octahedral and tetrahedral sites, the distribution of paramagnetic impurities, and the presence of crystallographically distinct Al sites.[15−19]

$^{17}$O NMR spectroscopy is also an effective structural probe of aluminosilicate materials, revealing, for instance, local site connectivity (e.g., $^{[4]}$Si−O−$^{[4]}$Si and $^{[4]}$Si−O−$^{[4]}$Al) and oxygen site-specific reactivity, but such studies of layer silicates are very limited.[20−22] In their pioneering study of synthetic talc [$Mg_3Si_4O_{10}(OH)_2$], Walter et al. used conventional static $^{17}$O NMR spectroscopy and static proton cross polarization ($^1$H−$^{17}$O static CP) to probe the oxygen environments.[20] More recently, we reported $^{17}$O triple-quantum magic-angle spinning (3QMAS) NMR spectra for $^{17}$O-enriched natural kaolinite and muscovite that provide improved resolution of the signal for the apical oxygens and, particularly, three crystallographically distinct basal oxygen sites in kaolinite, providing further insight into the origin of possible reactivity differences among the sites,[21] as previously demonstrated for zeolites, where $^{[4]}$Si−O−$^{[4]}$Al reacts more rapidly than $^{[4]}$Si−O−$^{[4]}$Si with $H_2O$ vapor.[23,24] $^{17}$O NMR studies of layer silicates are limited, largely because the NMR-active isotope, $^{17}$O, has a natural abundance of only 0.037%, and its relatively large quadrupolar moment can broaden the resonances through interactions with the electric field gradient (EFG).

Here, we use $^{17}$O and $^{27}$Al MAS and triple-quantum filtered MAS (3QMAS) NMR spectroscopies at various static magnetic fields ($H_0$) to explore the short-range cation order and O-site characteristics in three $^{17}$O-enriched synthetic layer silicates and $^{17}$O-enriched natural muscovite and kaolinite. Excellent resolution in the $^{17}$O 3QMAS NMR spectra at high field (14.1 T) allows previously unattainable discrimination of signals for multiple basal and apical oxygen sites, and the data provide the NMR characteristics of these sites. These results and methods provide a basis for future investigations of the oxygen sites in complex and heterogeneous nanomaterials. 3QMAS $^{17}$O NMR spectroscopy has previously proven effective in investigating the structures of crystalline oxide-based materials, including zeolites and aluminosilicate glasses.[23−30] Here, we use the FAM (fast amplitude modulation) modified pulse sequence, which can enhance the efficiency in triple quantum to single quantum conversion relative to that achieved with early methods.[24,31−33]

**Table 1. Synthetic Layer Silicate Samples**

| sample name | starting composition | final products |
|---|---|---|
| CAW1974 | kaolinite | kaolinite + smectite |
| CAW1964 | pyrophyllite | pyropyllite + kaolinite |
| CAW1961 | pyrophyllite | pyropyllite + kaolinite |

$^{27}$Al MAS NMR spectroscopy has been widely used to investigate the Al sites in layer silicates and to quantify the Al distribution between tetrahedral and octahedral layers, but principally because of second-order quadrupolar interactions (SQIs), such quantification has sometimes proven difficult (see ref 5 and references therein). Higher fields can reduce these difficulties,[34−36] and analysis of spinning sideband manifolds under fast MAS can provide a better method of obtaining structurally relevant quadrupolar coupling constants ($C_q$) and isotropic chemical shifts ($\delta_{iso}$).[16,37,38] Here, we use these techniques and $^{27}$Al 3QMAS to determine improved NMR parameters for layered silicates.

## Experimental Section

**Sample Preparation and Characterization.** Three $^{17}$O-enriched layer silicate samples (CAW1961, CAW1964, and CAW1974; see Table 1) were synthesized hydrothermally from gels using methods described previously.[39] Stoichiometric aliquots of $Al(NO_3)_3$ and TEOS (tetraethyl orthosilicate) were gelled in an excess of $NH_4(OH)$ and then dried at 50 °C. The dried gels were then crushed with a mortar and pestle. XRD analysis showed that they were amorphous. The layer silicates were synthesized hydrothermally[40] by reaction of a portion of gel with excess 46%-enriched $^{17}$O water in a sealed gold tube for 1 month at 350 °C and 1 kbar. Powder X-ray diffraction of the final products shows that they are mixtures of crystalline layer silicates (Figure 1). Samples CAW1961 and CAW1964 had initial bulk compositions equivalent to that of pyrophyllite

(11) Lausen, S. K.; Lindgreen, H.; Jakobsen, H. J.; Nielsen, N. C. *Am. Mineral.* **1999**, *84*, 1433−1438.
(12) Dekany, I.; Turi, L.; Fonseca, A.; Nagy, J. B. *Appl. Clay Sci.* **1999**, *14*, 141−160.
(13) Kinsey, R. A.; Kirkpatrick, R. J.; Hower, J.; Smith, K. A.; Oldfield, E. *Am. Mineral.* **1985**, *70*, 537−548.
(14) Weiss, C. A.; Altaner, S. P.; Kirkpatrick, R. J. *Am. Mineral.* **1987**, *72*, 735−742.
(15) Schroeder, P. A.; Pruett, R. J. *Am. Mineral.* **1996**, *81*, 26−38.
(16) Rocha, J.; Pedrosa de Jesus, J. D. *Clay Miner.* **1994**, *29*, 287−291.
(17) Kentgens, A. P. M. *Geoderma* **1997**, *80*, 271−306.
(18) Sanz, J.; Robert, J. L. *Phys. Chem. Miner.* **1992**, *19*, 39−45.
(19) de la Caillerie, J. B. D.; Man, P. P.; Vicente, M. A.; Lambert, J. F. *J. Phys. Chem. B.* **2002**, *106*, 4133−4138.
(20) Walter, T. H.; Turner, G. L.; Oldfield, E. *J. Magn. Reson.* **1988**, *76*, 106−120.
(21) Lee, S. K.; Stebbins, J. F. *Am. Mineral.* **2003**, *88*, 493−500.
(22) Brenn, U.; Ernst, H.; Freude, D.; Herrmann, R.; Jähnig, R.; Karge, H. G.; Kärger, J.; König, T.; Mädler, B.; Pingel, U.-T.; Prochnow, D.; Schwieger, W. *Microporous Mesoporous Mater.* **2000**, *40*, 43−52.
(23) Xu, Z.; Stebbins, J. F. *Geochim. Cosmochim. Acta* **1998**, *62*, 1803−1809.
(24) Zhao, P.; Neuhoff, P. S.; Stebbins, J. F. *Chem. Phys. Lett.* **2001**, *344*, 325−332.
(25) Dirken, P. J.; Kohn, S. C.; Smith, M. E.; van Eck, E. R. H. *Chem. Phys. Lett.* **1997**, *266*, 568−574.
(26) Pingel, U. T.; Amoureux, J. P.; Anupold, T.; Bauer, F.; Ernst, H.; Fernandez, C.; Freude, D.; Samoson, A. *Chem. Phys. Lett.* **1998**, *294*, 345−350.
(27) Cheng, X.; Zhao, P. D.; Stebbins, J. F. *Am. Mineral.* **2000**, *85*, 1030−1037.
(28) Lee, S. K.; Stebbins, J. F. *J. Non-Cryst. Solids.* **2000**, *270*, 260−264.
(29) Lee, S. K.; Stebbins, J. F. *Geochim. Cosmochim. Acta* **2002**, *66*, 303−309.
(30) Lee, S. K.; Stebbins, J. F. *J. Phys. Chem. B.* **2000**, *104*, 4091−4100.
(31) Kentgens, A. P. M.; Verhagen, R. *Chem. Phys. Lett.* **1999**, *300*, 435−443.
(32) Madhu, P. K.; Goldbourt, A.; Frydman, L.; Vega, S. *Chem. Phys. Lett.* **1999**, *307*, 41−47.
(33) Vosegaard, T.; Massiot, D.; Grandinetti, P. J. *Chem. Phys. Lett.* **2000**, *326*, 454−460.
(34) Kohn, S. C.; Smith, M. E.; Dirken, P. J.; van Eck, E. R. H.; Kentgens, A. P. M.; Dupree, R. *Geochim. Cosmochim. Acta* **1998**, *62*, 79−87.
(35) Stebbins, J. F.; Kroeker, S.; Lee, S. K.; Kiczenski, T. J. *J. Non-Cryst. Solids* **2000**, *275*, 1−6.
(36) Lee, S. K.; Stebbins, J. F. *Geochim. Cosmochim. Acta* **2003**, *67*, 1699−1709.
(37) Skibsted, J.; Nielsen, N. C.; Bildsøe, H.; Jakobsen, H. J. *J. Magn. Reson.* **1991**, *95*, 88−117.
(38) Jäger, C. In *Solid State NMR II: Inorganic Matter*; Diehl, P., Fluck, E., Günther, H., Kosfeld, R., Seelig, J., Eds.; Springer-Verlag: Berlin, 1994; Vol. 31, pp 135−170.
(39) Luth, W. C.; Ingamells, C. O. *Am. Mineral.* **1965**, *50*, 255−258.
(40) Eberl, D.; Hower, J. *Clay Clay Miner.* **1975**, *23*, 301−309.

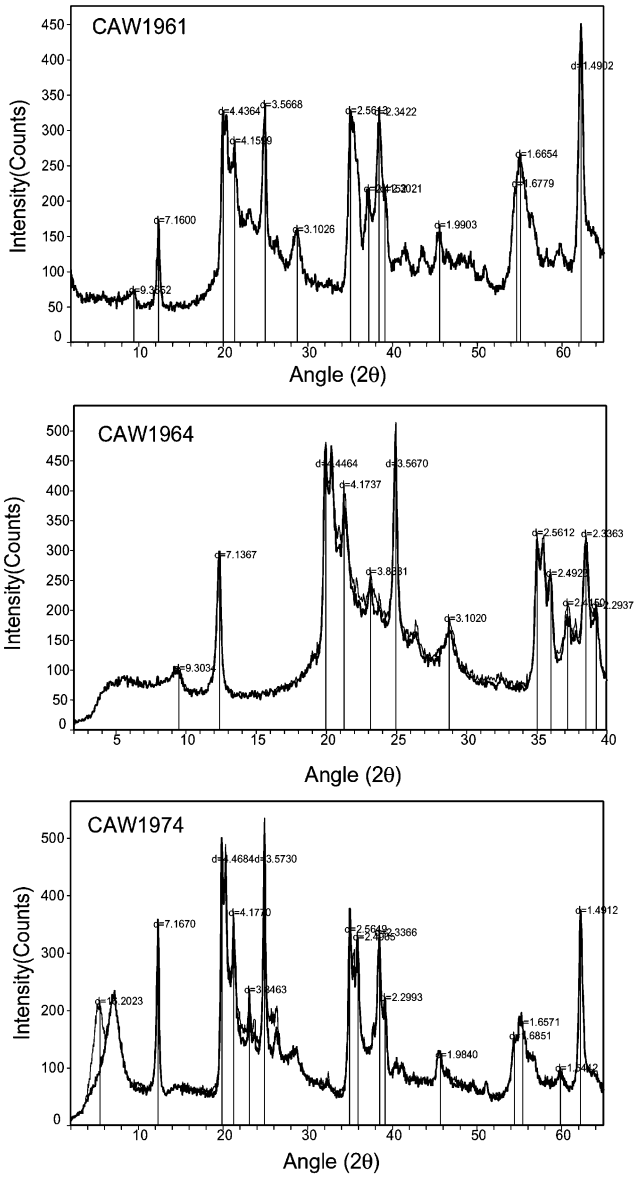


**Figure 1.** X-ray diffraction data for synthetic layer silicates. The thin line shows the data for ethylene glycol-treated samples to check the presence of expandable layers.

(Al/Si = 2) and produced a mixture of pyrophyllite and kaolinite. Sample CAW1974 had an initial bulk composition equivalent to that of kaolinite (Al/Si = 1) and produced a mixture of kaolinite and expandable smectite. The fraction of each phase is difficult to quantify. These samples might also contain residual amorphous material, as suggested by the broad diffraction peaks spanning 20−30° 2$\theta$. If an amorphous phase is present, it must be nearly pure (hydrous) silica, as the $^{27}$Al NMR data contain no signal attributable to it. The formation of expandable smectite in CAW1974 is unexpected because of the kaolinite composition and might be due to the presence of $NH^{4+}$ in the starting reaction mixture.[41]

Preparation and characterization of the $^{17}$O-enriched natural samples is described in our previous report.[21] Briefly, 150 mg of muscovite powder from Maine (Stanford University mineral collection #62780) was mixed with an equal mass of 46% $^{17}$O-enriched water and reacted at 773 K and 1 kbar for 1 month in a sealed gold tube in a cold seal hydrothermal vessel. Standard Georgia kaolinite (KGa-1b, from the Clay Minerals Society Source Clay Repository, hereafter called kaolinite_Ga) was reacted with an equal mass of 46% $^{17}$O-enriched water at 573 K and 200 bar for 1 month in an approach similar to that used with muscovite.[21] KGa-1b was well-characterized,[42] and the $^{17}$O-enriched kaolinite_Ga contained no alteration products or evidence of dissolution−recrystallization detectable by SEM with EDX or by $^{27}$Al MAS NMR spectroscopy at 14.1 T.

**NMR Spectroscopy.** *$^{17}$O NMR Spectroscopy.* The $^{17}$O NMR spectra were obtained with three spectrometers at magnetic fields of 9.4, 14.1, and 18.8 T. At 14.1 and 18.8 T, data were collected using Varian INOVA 600 and Varian INOVA 800 systems at Larmor frequencies of 81.31 MHz (14.1 T) and 108.4 MHz (18.8 T), respectively. Varian/Chemagnetics T3 MAS probes (3.2 mm) with spinning speeds of 18 and 20 kHz were used at 14.1 and 18.8 T, respectively. Relaxation delays were 1 s with pulse lengths of 0.15 (14.1 T) and 0.2 ms (18.8 T). The $^{17}$O 3QMAS NMR spectra at 14.1 T were collected using an FAM-based,[24,31−33] shifted-echo pulse sequence composed of pulses of 3 and 0.7 ms for triple quantum excitation and single quantum reconversion, respectively, and a selective pulse with a duration of 20 ms with varying delay times depending on the spin−lattice relaxation time of the samples with a spinning speed of 18 kHz.

The $^{17}$O MAS and 3QMAS spectra at 9.4 T were collected with a modified Varian VXR-400S spectrometer at a Larmor frequency of 54.22 MHz, using a 5-mm Doty scientific MAS probe at a spinning speed of 15 kHz. Recycle delays ranged from 1 to 15 s with radio-frequency pulse lengths of 0.3 ms (about 15° tip angle for the central transition in solids). The FAM-based shifted-echo pulse sequence comprising hard pulses with durations of 5.2 and 1.7 $\mu$s, a selective pulse with a duration of 26 $\mu$s, and an echo time of an integer multiple of the rotor period was used. Static Hahn-echo ("nonspinning") NMR spectra were collected for sample CAW1964 to examine the spin−spin relaxation time ($T_2$) of the oxygen sites using two pulses of 13 $\mu$s ($\pi$/2) and 26 $\mu$s ($\pi$) and varying echo times with a recycle delay of 0.3 s. The $^{17}$O NMR spectra are referenced to external tap water (9.4 T) and $^{17}$O-enriched water (14.1 and 18.8 T). 3QMAS data were processed with a shear transformation, with the isotropic dimension frequencies scaled as described previously.[43]

*$^{27}$Al NMR Spectroscopy.* $^{27}$Al 3QMAS NMR spectra at 9.4 T (104.22 MHz) and 14.1 T (156.28 MHz) were collected with the shifted-echo pulse sequence described previously,[28,30,43] with spinning rates of 14 kHz (9.4 T) and 18k Hz (14.1 T) and recycle delays of 1 s. $^{27}$Al MAS NMR spectra at 14.1 T were collected with recycle delays of 1 s and a radio-frequency pulse length of 0.23 $\mu$s, which is approximately a 15° tip angle for the central transition in solids. Peak positions were reported relative to external 1 M aqueous $Al(NO_3)_3$. MAS spinning sidebands for $^{27}$Al were simulated with the STARS software package (Varian Inc.) The effect of preferred orientation on NMR spectra was previously found to be negligible.[21]

## Results and Discussion

**$^{17}$O MAS NMR Results.** Each of the samples studied yields distinctive $^{17}$O MAS NMR spectra at 9.4 and 14.1T, and although resolution of different oxygen sites is better at 14.1 T, even this field is insufficient to allow discrimination of crystallographically distinct oxygen sites or to determine the NMR parameters for each oxygen site from MAS spectra alone (Figure 2). Dioctahedral (2:1) layer silicates contain several types of oxygens (apical $2^{[6]}$Al−O−$^{[4]}$Si, basal $^{[4]}$Si−O−$^{[4]}$Si, basal $^{[4]}$Si−O−$^{[4]}$Al, and oxygens in hydroxyl groups), as illustrated in Figure 3 for pyrophyllite [$Al_2Si_2O_{10}O$-$(OH_2)$]. The poor resolution in our MAS spectra is due to a combination of spectral broadening caused by

(41) Brindly, G. W., Brown, G., Eds. *Crystal Structure of Clay Minerals and Their X-ray Identifcation*; Mineralogical Society: London, 1980.

(42) de Ligny, D.; Navrotsky, A. *Am. Mineral.* **1999**, *84*, 506−516.

(43) Baltisberger, J. H.; Xu, Z.; Stebbins, J. F.; Wang, S.; Pines, A. *J. Am. Chem. Soc.* **1996**, *118*, 7209−7214.

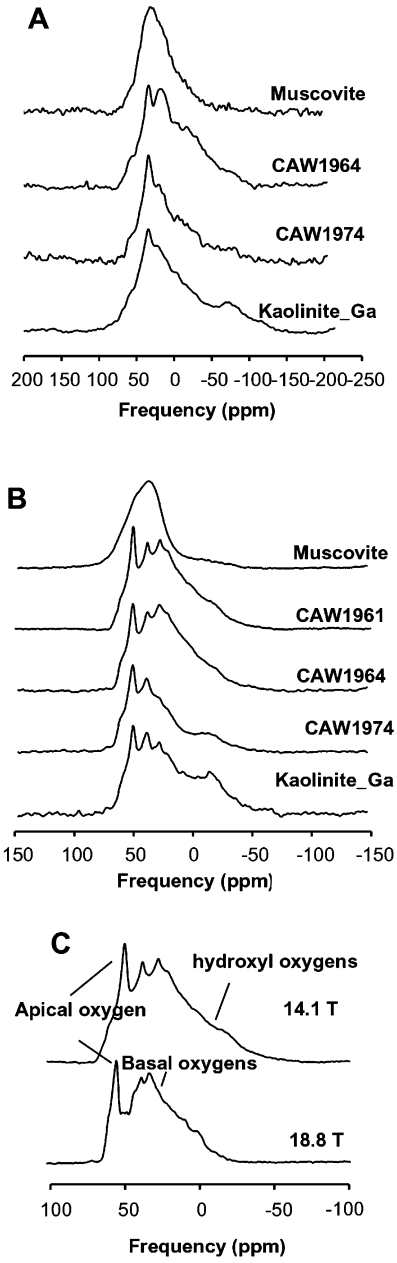


**Figure 2.** $^{17}$O MAS NMR spectra for the indicated layer silicates at (A) 9.4 and (B) 14.1 T, and (C) comparison of spectra at 14.1 and 18.8 T for sample CAW1961.

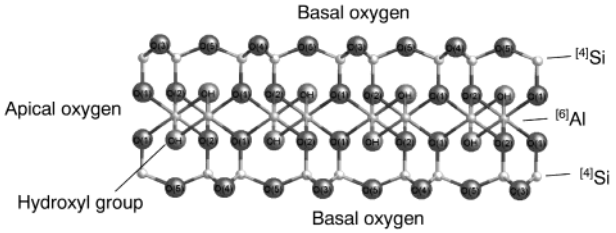


**Figure 3.** Structure of pyrophyllite illustrating apical, basal, and hydroxyl group oxygen sites.

unaveraged second-order quadrupolar effects (SQI, which decreases with increasing $H_0$ field strength) and the similarity of the NMR responses of some sites.[19] The resonances for muscovite might be further broadened by the presence of paramagnetic impurities or possible Si−Al disorder in the tetrahedral layers. The observed resonances can be assigned on the basis of previous studies.[20,44,45] The sharp peak near 50 ppm is due to apical 2[6]Al−O−[4]Si sites that link the tetrahedral and octahedral layers. The group of overlapping resonances between 0 and 45 ppm is due to multiple basal oxygen sites.[21] Broad features in the lower-frequency shoulder of the spectra (at negative chemical shifts) are due to hydroxyl groups with relatively large $C_q$ values of about 7 MHz, consistent with previous studies of hydroxyl groups in talc and silica gel.[20,44,45] CAW1961 and CAW1964 show higher intensity than the other samples near 30 ppm, possibly due to [4]Si−O−[4]Si in residual amorphous material or basal oxygens with relatively large [4]Si−O−[4]Si angles in pyrophyllite (see discussion below).

Resolution of apical and basal oxygen sites is improved at 18.8 T, as shown in our previous study of kaolinite[21] and the data for sample CAW1961 (Figure 2C here). With increasing $H_0$ field, the peak position of each oxygen site moves toward higher frequency because of reduced SQI. Resolution of basal and hydroxyl sites does not improve, however, because these sites have similar $^{17}$O isotropic chemical shift ($\delta_{iso}$) ranges and relatively large $C_q$ values. For example, $\delta_{iso}$ of the basal oxygens in kaolinite ranges from 46.5 to 54.3 ppm with a $C_q$ of about 4.65 MHz, whereas the corresponding values for hydroxyl groups are about 41.5 ppm and 6.9 MHz.[21]

*$^{17}$O 3QMAS NMR Results.* $^{17}$O 3QMAS NMR spectra provide a significant improvement in resolution (Figure 4), especially among basal and apical oxygen sites, because of averaging of the SQI in the isotropic dimension. Peak positions in this dimension, however, are related to both $\delta_{iso}$ and the second-order quadrupolar shift.[46] For the $^{17}$O-enriched natural muscovite, two different types of basal oxygens, [4]Si−O−[4]Si and [4]Si−O−[4]Al (required by the presence of Al in the tetrahedral layers), are well-resolved, whereas they cannot be distinguished by $^{17}$O MAS NMR spectroscopy. In contrast, the apical oxygens are somewhat less well resolved from [4]Si−O−[4]Si. Signal for the hydroxyl groups can be detected at negative chemical shifts. The 3QMAS NMR spectrum of CAW1974 shows higher resolution of the same types of sites, probably because of the absence of paramagnetic impurities. The apical and basal oxygens are well-resolved in this spectrum. [4]Si−O−[4]Al is again due to Al substitution in the tetrahedral layer, which is the source of the permanent negative layer charge for the expandable smectite observed by XRD (Figure 1). Careful examination indicates the presence of at least two types of [4]Si−O−[4]Si sites, as expected by the presence of both kaolinite and smectite in the sample. The 2[6]Al−O−H peak is difficult to observe in this spectrum because of the relatively rapid $T_2$ relaxation of the hydroxyl oxygen (see below) and its large $C_q$. The relatively large radio-frequency field strength in this study (122 kHz) and the large fraction of oxygens on hydroxyl sites in 2:1 dioctahedral layer silicates (17%), however, allow detection of some signal from them here.[21,44]

(44) van Eck, E. R. H.; Smith, M. E.; Kohn, S. C. *Solid State NMR* **1999**, *15*, 181−188.
(45) Walter, T. H.; Oldfield, R. *J. Phys. Chem.* **1989**, *93*, 6744−6751.
(46) Frydman, I.; Harwood, J. S. *J. Am. Chem. Soc.* **1995**, *117*, 5367−5368.

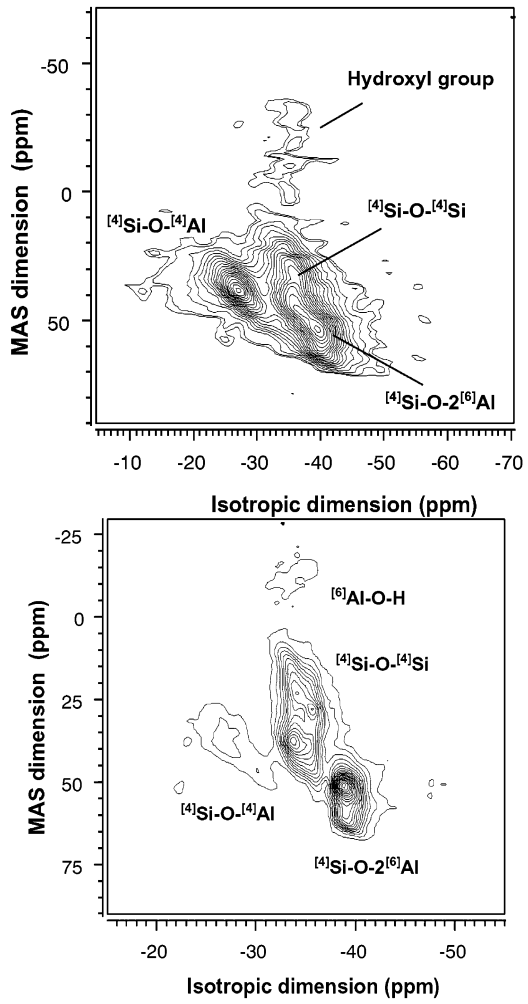


**Figure 4.** $^{17}$O 3QMAS NMR spectra of enriched natural muscovite (top) and CAW1974 (bottom) at 14.1 T. The structurally relevant NMR parameters such as quadrupolar coupling constant ($P_q$) and isotropic chemical shifts ($\delta_{iso}$) from the approximate peak positions of basal and apical oxygens are as follows. Peak positions and NMR parameters of each peak are given in the order $\delta_{MAS}$, $\delta_{3QMAS}$, $C_q$, $\delta_{iso}$, assuming an asymmetry parameter ($\eta$) of 0. Muscovite: $^{[4]}$Si−O−$^{[4]}$Si ($\delta_{MAS}$ = 35 ppm, $\delta_{3QMAS}$ = −35 ppm, $C_q$ = 4.5 MHz, $\delta_{iso}$ = 53.2 ppm), $^{[4]}$Si−O−$^{[4]}$Al (37.6 ppm, −27.5 ppm, 2.89 MHz, 45.22 ppm), $^{[4]}$Si−O−2$^{[6]}$Al (55 ppm, −40 ppm, 3.5 MHz, 66.3 ppm), 2$^{[6]}$Al−OH (−15 ppm, −34.8 ppm, 7.4 MHz, 34 ppm). CAW1974: $^{[4]}$Si−O−$^{[4]}$Si (I) (31 ppm, −34 ppm, 4.6 MHz, 50.5 ppm), $^{[4]}$Si−O−$^{[4]}$Si (II) (35 ppm, −36 ppm, 4.6 MHz, 54 ppm), $^{[4]}$Si−O−$^{[4]}$Al (36 ppm, −27 ppm, 3 MHz, 44.3 ppm), $^{[4]}$Si−O−2$^{[6]}$Al (55 ppm, −39.5 ppm, 3.4 MHz, 65.7 ppm), 2$^{[6]}$Al−OH (−14 ppm, −33.4 ppm, 7.2 MHz, 33.2 ppm). See Figure 9 for NMR parameters obtained from simulations of MAS NMR spectra using the parameters obtained from peak position in 3QMAS NMR spectra as initial guesses.

A comparison of the spectra obtained at 9.4 and 14.1T for sample CAW1964 demonstrates the greatly improved resolution in $^{17}$O 3QMAS NMR spectra at higher $H_0$ fields (Figure 5). Apical and basal oxygens are not well resolved at 9.4 T, whereas the 14.1-T spectrum clearly shows at least four or five $^{[4]}$Si−O−$^{[4]}$Si sites and well-resolved apical oxygen. No $^{[4]}$Si−O−$^{[4]}$Al sites are expected for this sample, because XRD shows that it contains only pyrophyllite and kaolinite, neither of which contain $^{[4]}$Al. In general, $^{17}$O 3QMAS NMR spectroscopy at high fields more effectively resolves sites with similar quadrupolar coupling products, $P_q$, and $\delta_{iso}$,

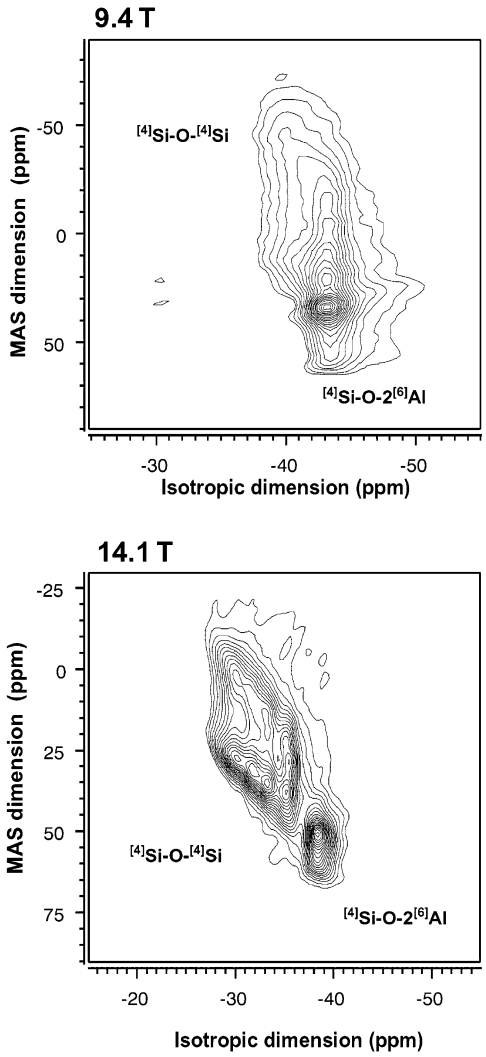


**Figure 5.** $^{17}$O 3MAS NMR spectra for CAW1964 at 9.4 (top) and 14.1 T (bottom). Peak positions (see Figure 6 for leveling) and NMR parameters of each peak are given in the order $\delta_{MAS}$, $\delta_{3QMAS}$, $C_q$, $\delta_{iso}$, assuming an asymmetry parameter ($\eta$) of 0. CAW1964: $^{[4]}$Si−O−$^{[4]}$Si (A) (31.7 ppm, −35.3 ppm, 4.2 MHz, 52.2 ppm), $^{[4]}$Si−O−$^{[4]}$Si (B) (26.9 ppm, −33.3 ppm, 4.9 MHz, 48.2 ppm), $^{[4]}$Si−O−$^{[4]}$Si (C) (20.8 ppm, −31.8 ppm, 5.1 MHz, 44.12 ppm), $^{[4]}$Si−O−$^{[4]}$Si (D) (15 ppm, −30 ppm, 5.2 MHz, 40 ppm), $^{[4]}$Si−O−$^{[4]}$Si (E) (10 ppm, −28.6 ppm, 5.5 MHz, 36 ppm), $^{[4]}$Si−O−2$^{[6]}$Al (54 ppm, −38.5 ppm, 3.4 MHz, 64.2 ppm).

whereas low-field 3QMAS NMR spectroscopy more effectively resolves sites with different $C_q$'s. Here, $P_q = C_q(1 + \eta^2/3)^{1/2}$, where $0 \leq \eta \leq 1$ is the quadrupolar asymmetry parameter. $\delta_{iso}$ can be obtained from the center of gravity of the peak in 3QMAS NMR spectra.[43]

Projection of the signal onto the isotropic dimension of $^{17}$O 3QMAS spectra (the so-called total isotropic projection) often provides important structural information, because of the absence of second-order quadrupolar effects on the peak shape, as illustrated in Figure 6 for samples CAW1964, CAW1974, and kaolinite_Ga. Their spectra are consistent with our previous results that apical oxygens sites have smaller $C_q$'s and larger isotropic chemical shifts than basal oxygens, and that hydroxyl group oxygens have an isotropic chemical shifts similar to that of basal oxygens but have larger $C_q$'s. These results for the $^{17}$O-enriched natural kaolinite were discussed previously.[21] For this sample, the peaks for the two apical oxygens with slightly different Si−O

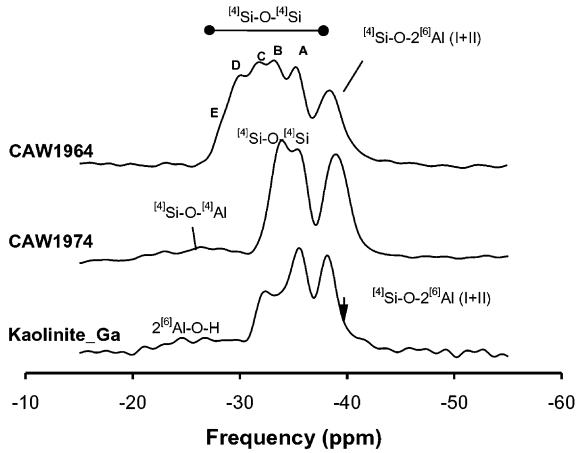


**Figure 6.** Total projections in the isotropic dimension of $^{17}O$ 3QMAS spectra for two synthetic layer silicates and kaolinite at 14.1 T. The isotropic projection of kaolinite was previously reported.[21]

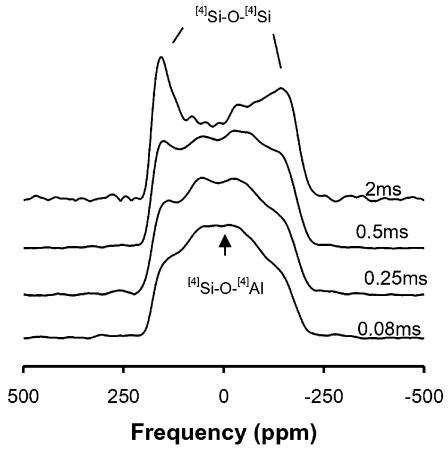


**Figure 7.** $^{17}O$ Hahn-echo static NMR spectra of CAW1964 at 9.4 T with varying echo times as labeled.

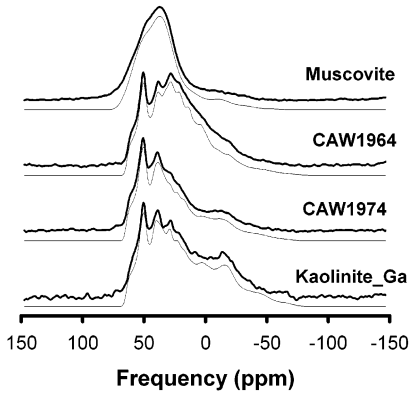


**Figure 8.** Fitting results for $^{17}O$ MAS NMR spectra for layer silicates at 14.1 T. Thin lines refer to results simulated using the $C_q$ and $\delta_{iso}$ from $^{17}O$ 3QMAS NMR spectroscopy as initial parameters. Thick lines are observed spectra.

and Al−O bond lengths occur at −38 (main peak) and −39 ppm (arrow) in the total isotropic projection and are narrower than the same peaks for the other samples. The peak positions for the three basal oxygen sites are similar to A, B, and C in the CAW1964. These three peaks reflect three crystallographically distinct sites with different Si−O−Si angles in the natural kaolinite (see below for peak assignment and ref 21 for detailed information).

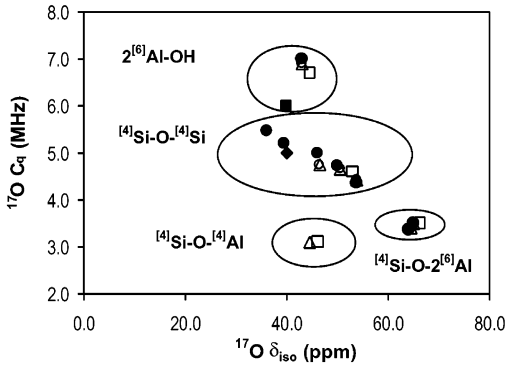


**Figure 9.** $^{17}O$ $C_q$ and $\delta_{iso}$ ranges of each oxygen site in layer silicates. The closed and open circles are for CAW1964 and kaolinite_Ga, respectively. The closed and open squares refer to the NMR parameters of bayerite[45] and natural muscovite,[21] respectively. The closed circle is for the NMR parameters of boehmite.[45] Open triangles are $^{17}O$ $C_q$ and $\delta_{iso}$ results for CAW1974. Larger ellipses suggest the ranges of the NMR parameters for layer silicates.

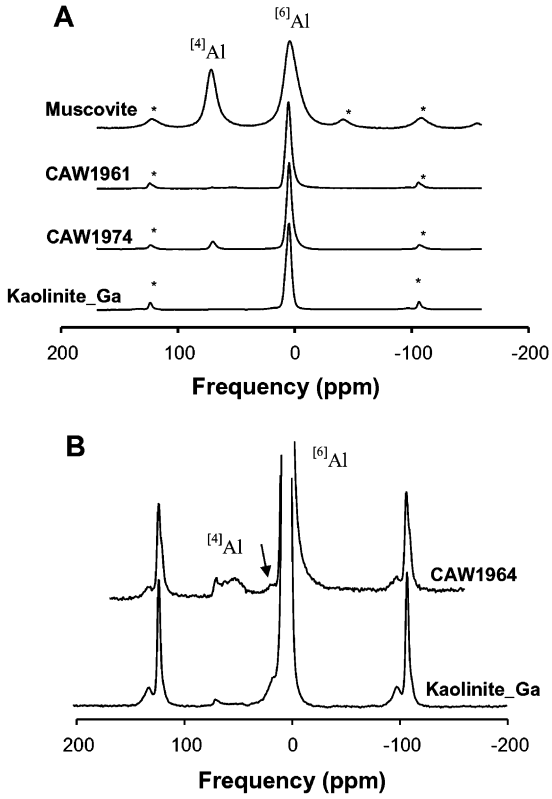


**Figure 10.** $^{27}Al$ MAS NMR spectra for layer silicates at 14.1 T. The asterisks (*) show the spinning sidebands.

The total isotropic projection for CAW1974 shows a poorly resolved signal for apical sites about −39 ppm, two resolved peaks for [4]Si−O−[4]Si (peak positions similar to A and B in CAW1964), and [4]Si−O−[4]Al (broad peak at −26 ppm) due to oxygen sites in smectite, as discussed above (Figure 6). The [4]Si−O−[4]Si signals are due to these sites in both kaolinite and smectite, but assignment is difficult: Kaolinite_Ga contains three crystallographically distinct basal oxygen sites, but the structures of smectites are poorly understood in detail. The intensity of the peak at −32 ppm in the isotropic dimension (peaks C) is smaller for CAW1974 than for kaolinite_Ga, possibly because of differences in the kaolinite polytype. However, it is also possible that the

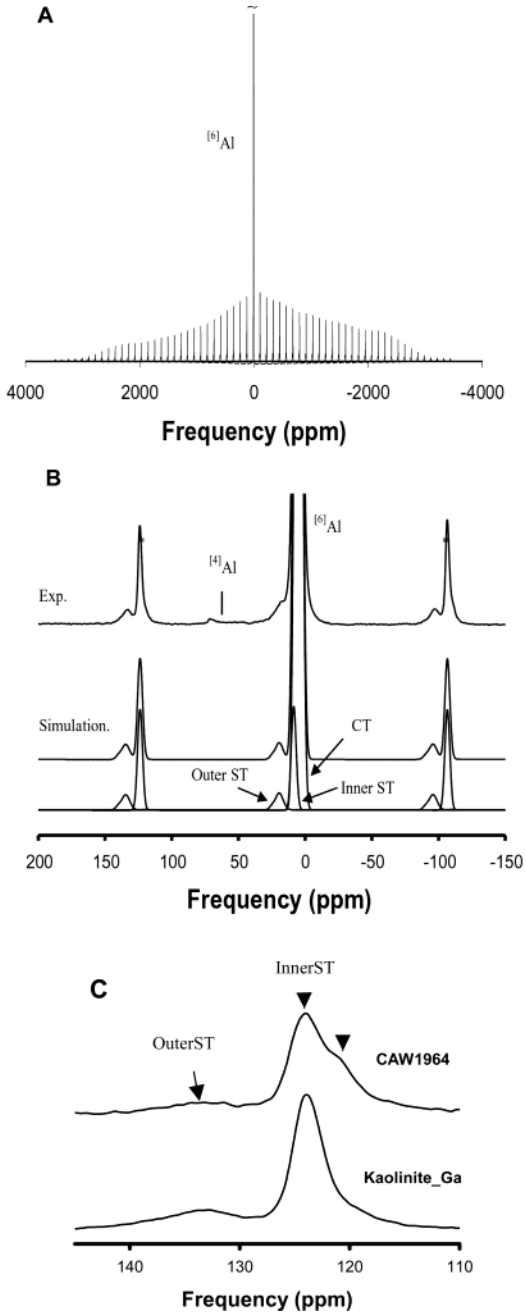


**Figure 11.** (A) Spinning sideband manifold of $^{27}$Al MAS spectra for kaolinite. (B) Simulation of the satellite spinning sidebands and central transition (CT) of kaolinite. ST denotes satellite transitions (outer ST $\{\pm^5/_2 - \pm^3/_2\}$, inner ST $\{\pm^3/_2 - \pm^1/_2\}$). (C) Details of the SSB patterns for kaolinite and CAW1964.

relative peak intensities for the natural kaolinite do not represent true crystallographic site populations because of differences in the reactivity among oxygen sites.

The 14.1-T $^{17}$O 3QMAS spectrum of CAW1964, which contains both kaolinite and pyrophyllite, exhibits a broad peak for apical oxygens at about −39 ppm and four or five peaks for basal $^{[4]}$Si−O−$^{[4]}$Si sites (labeled A−E in Figure 6). Unique quantitative structural assignment of these peaks is not currently possible, because the relationships between structure (principally Si−O−Si bond angle) and NMR parameters remain uncertain, and because the differences in bond angles and lengths among the crystallographically distinct basal oxygen sites of kaolinite and pyrophyllite are small. In addition, the proportions of the phases in the synthetic samples are not known. Qualitative assessment will, however, be useful in future spectral analysis. The three relatively low-frequency peaks for CAW1964 (A, B, and C) appear to be similar to the peaks for the basal oxygen sites in kaolinite, as discussed above.[21] The higher-frequency (less negative in the isotropic projection) sites D, E, and some part of C, which occur for only CAW1964 might be related to the three basal oxygen sites of pyrophyllite. This would explain the absence of sites D and E in the total isotropic projection of kaolinite (see below). NMR data for pure minerals including pyrophyllite would be helpful for further quantification of such results.

**$^{17}$O Hahn-Echo Static NMR Spectra for CAW1964.** Quantitative signal intensity interpretation of $^{17}$O 3QMAS NMR spectra is sometimes possible if the 3QMAS efficiency (which depends on $C_q$ and experimental conditions) is carefully calibrated using standards.[30,36] Such interpretations for layer silicates are complicated, however, by potentially different $T_2$ relaxation times for different oxygen sites due, perhaps, to different distances from the protons of hydroxyl groups or dipolar and quadrupolar interactions between $^{17}$O and other nuclei. This effect is well illustrated by the 9.4-T $^{17}$O static Hahn-echo NMR spectra of synthetic sample CAW1964 obtained with varying echo times (Figure 7). These spectra provide NMR signal free from probe ringing, including information regarding the dephasing time of the different sites. With increasing echo time, the intensity of the $^{[4]}$Si−O−$^{[4]}$Si signal (doublet with larger width, $C_q$ of about 4.5−5 MHz) increases, whereas the signal for $^{[4]}$Si−O−$^{[4]}$Al (central region, $C_q$ of about 3.5 MHz) becomes less prominent. This must be due to a shorter $T_2$ value for $^{[4]}$Si−O−$^{[4]}$Al. 3QMAS experiments involve manipulation of spin−echos, and thus, the intensities of sites with with smaller $T_2$ values are likely to be underestimated, as recently observed for silica gel.[44]

**Peak Assignment and NMR Characteristics of Oxygen Sites in Layer Silicates.** As discussed above and in our previous study,[21] assigning the $^{17}$O peaks for the various basal oxygen sites in layer silicates is challenging because differences in the bond lengths and angles of crystallographically distinct sites are relatively small and because there is uncertainty in the correlations between NMR parameters and structure. Previous quantum chemical calculations and $^{17}$O NMR data for crystalline coesite ($SiO_2$) suggest that the $^{17}$O $C_q$ of $^{[4]}$Si−O−$^{[4]}$Si sites increases with increasing $^{[4]}$Si−O−$^{[4]}$Si angle,[47] but other studies of zeolites do not show this simple trend.[48]

Simulation of the 14.1-T $^{17}$O MAS NMR spectra of our samples using the NMR parameters ($P_q$ and $\delta_{iso}$) for most sites from the 3QMAS NMR spectra (these parameters are given in the captions of Figures 4 and 5) provides important insight into the relationships for $^{[4]}$Si−O−$^{[4]}$Si sites in layer silicates (Figure 8). Fitting of the MAS spectra yields values for $C_q$ and $\eta$, which

(47) Grandinetti, P. J.; Baltisberger, J. H.; Farnan, I., Stebbins, J. F.; Werner, U.; Pines, A. *J. Phys. Chem.* **1995**, *99*, 12341−12348.
(48) Bull, L. M.; Bussemer, B.; Anupold, T.; Reinhold: A.; Samoson, A.; Sauer, J.; Cheetham, A. K.; Dupree, R. *J. Am. Chem. Soc.* **2000**, *122*, 4948−4958.

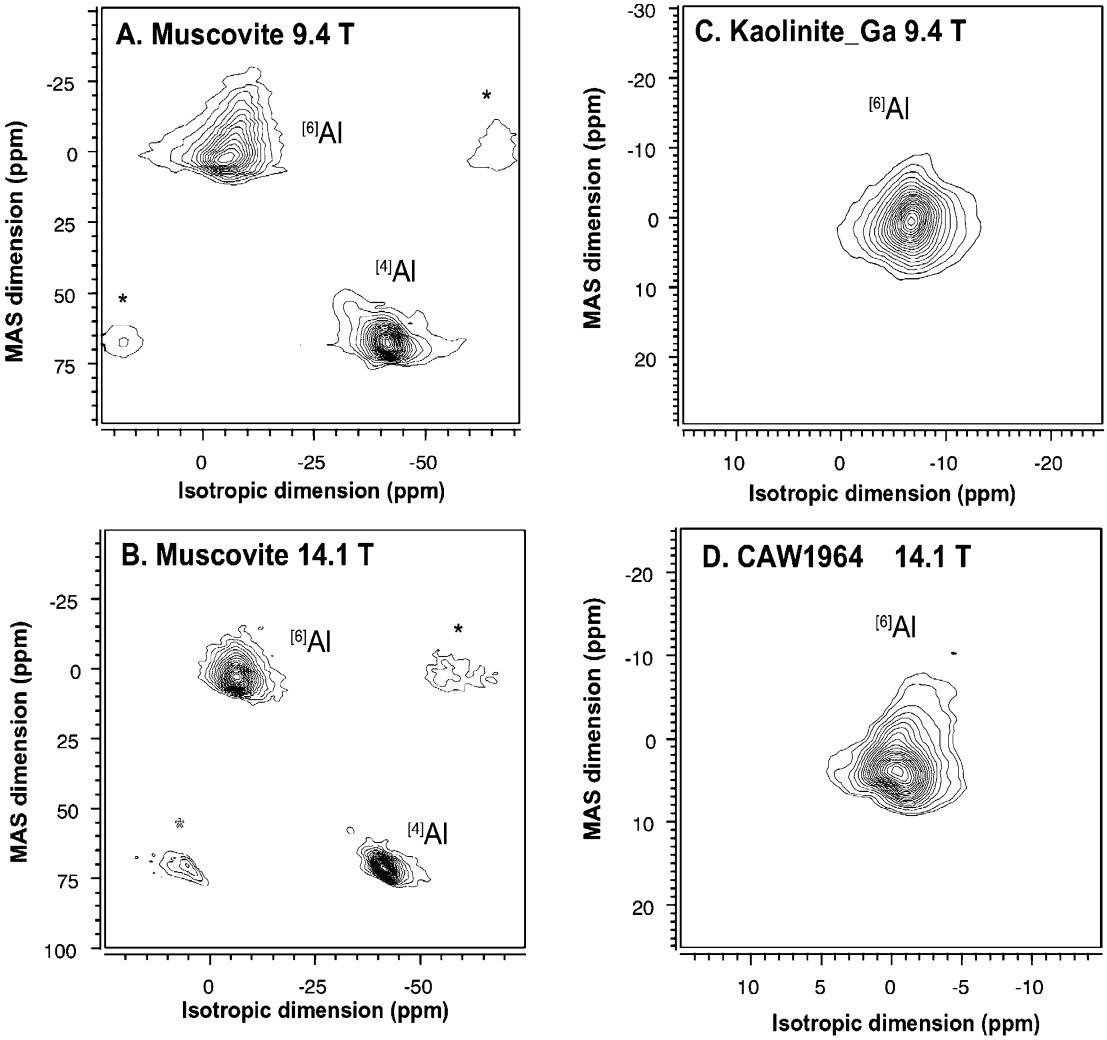


**Figure 12.** $^{27}$Al 3QMAS NMR spectra for muscovite at (A) 9.4 and (B) 14.1 T. Contour lines are drawn from 7 to 97% of total intensity with addition of a line at 5% intensity. (C) $^{27}$Al 3QMAS NMR spectra of natural kaolinite at 9.4 T and (D) CAW1964 at 14.1 T. The asterisks (*) denote spinning sidebands.

cannot be determined independently from the $P_q$ values of the 3QMAS spectra. The $C_q$ and $\eta$ NMR parameters for kaolinite were given in our previous publication and are the best constrained[21] because the sample is single-phase. The simulations for CAW1964, CAW1974, and muscovite are quite good but are nonunique and should be regarded as one possible solution. For CAW1964, we fitted five basal oxygen sites (A−E in Figure 6) to fully describe the spectrum.

The overall results show well-defined ranges of $\delta_{iso}$ and $C_q$ for $^{17}$O in our layer silicate samples (Figure 9). This figure also includes the NMR parameters for $^{17}$-OH in bayerite [$Al(OH)_3$] and boehmite [AlO(OH)] for comparison of the hydroxyl groups.[45] For the basal oxygens, $C_q$ increases with increasing $\delta_{iso}$, but we do not attempt to assign the peaks to crystallographic sites for the reasons described above. In our previous study,[21] we used the correlation of $C_q$ and bond angle for peak assignment of kaolinite,[47] leading to the assignment of the peak equivalent to peak C here to the site with largest bond angle (142.5°) and the peaks equivalent to peaks A and B (smaller $C_q$ and larger $\delta_{iso}$) to basal oxygen sites with smaller Si−O−Si angles (130.6° and 131.4°).[49] For pyrophyllite, the Si−O−Si angles for the three basal oxygen sites are all approximately 135−136°, making assignment using this correlation uncertain. Individual Si−O−Si and Si−O−Al bond angles are unknown for muscovite, because of tetrahedral Al−Si disorder. The quadrupolar asymmetry parameters, $\eta$, for apical oxygens and oxygens of hydroxyl groups are 0.8 (±0.05) and 0.5 (±0.2), respectively, and for the basal oxygens they vary from 0.2 to 0.5. More experiments with pure samples, in particular for pyrophyllite, are necessary to better constrain results for more complex systems.

**$^{27}$Al NMR Results.** The $^{27}$Al MAS NMR spectra of our samples obtained at 14.1 T support the structural interpretations from the $^{17}$O data and provide new, high-resolution results concerning the octahedral sites (Figure 10A). Muscovite yields both $^{[4]}$Al and $^{[6]}$Al peaks with an $^{[6]}$Al/$^{[4]}$Al ratio of 1.95 (±0.1), consistent with the ideal composition. The $^{27}$Al MAS NMR spectrum of CAW1974 shows unresolved $^{[6]}$Al for kaolinite and smectite and an additional 7−8% $^{[4]}$Al, consistent with the presence of $^{[4]}$Si−O−$^{[4]}$Al sites in the smectite inferred from the $^{17}$O 3QMAS NMR spectrum. Kaolinite_Ga and CAW1961 yield negligible fractions of $^{[4]}$Al. The $^{[6]}$Al peak widths of CAW1961 and CAW1974 are broader than that for kaolinite_Ga, probably because of the presence of two

(49) Bish, D.; Vondreele, R. B. *Clay Clay Miner.* **1989**, *37*, 289−296.

phases in the synthetic samples. The shoulder on the lower-frequency side of the $^{[6]}$Al peak might be due to a distribution of $C_q$ caused by structural disorder or overlap of signal from the two phases.

The intensity on the high-frequency side of the $^{[6]}$Al central transition peak (arrow in Figure 10B) is a satellite transition spinning sideband (SSB), as shown by a simulation including both the inner and outer satellite transitions (STs) (Figure 11B). (See ref 38 for more information.) Figure 11A shows the entire $^{27}$Al MAS NMR SSB manifold for kaolinite_Ga, and Figure 11B illustrates the SSB fitting results, including the contributions of the inner $\{\pm^3/_2 - \pm^1/_2\}$ and outer $\{\pm^5/_2 - \pm^3/_2\}$ ST SSBs. There is a good fit between the simulated and observed individual SSBs, but the simulated SSB manifold for the entire frequency range has more prominent singularities than the experimental data.[38] This discrepancy is probably not due to the effect of chemical shift anisotropy (CSA) and its interaction with the quadrupolar tensor, but rather to the off-resonance conditions for this experiment, as manifested in the asymmetry of the manifold. The $C_q$, $\delta_{iso}$, and $\eta$ values of $^{[6]}$Al in kaolinite from this analysis are 3.1 (±0.05) MHz, 8.1 (±0.3) ppm, and 0.95 (±0.05), respectively. These values are comparable to the results obtained from previous studies (e.g., $\delta_{iso} = 7$ (±1) ppm and $P_q = 3.6$ (±0.2) MHz[50]), but the values from the analysis of the SSB manifold are much more precise. A previously published analysis of the $^{27}$Al MAS NMR SSB manifold of a more ordered kaolinite obtained at 9.4 T showed the presence of two $^{[6]}$Al sites, one with $C_q = 3.53$, $\eta = 0.67$, and $\delta_{iso} = 8.9$ ppm and the other with $C_q = 2.89$ MHz, $\eta = 0.97$, and $\delta_{iso} = 7.8$ ppm.[16] The means of these values are similar to the values presented here. Even if our sample did contain two $^{[6]}$Al sites similar to these, it would be difficult to observe two signals in the inner ST sidebands for kaolinite_Ga because its crystallinity is lower than that of the sample used for the previous study (Figure 11C),[16] which leads to broader $^{[6]}$Al peak for kaolinte_Ga. The inner SSBs of CAW1964 do contain two features (Figure 11C), suggesting resolution of the $^{[6]}$Al sites from kaolinite and pyrophyllite.

To seek better resolution of the different $^{[6]}$Al sites in our samples, we applied $^{27}$Al 3QMAS NMR spectroscopy,[51] but separate sites were not observed. The 9.4- and 14.1-T $^{27}$Al 3QMAS NMR spectra of muscovite show only single $^{[4]}$Al and $^{[6]}$Al peaks, with better quantification of the $^{[6]}$Al/$^{[4]}$Al ratio at 14.1 T than at 9.4 T, as observed under MAS only (Figure 12A and B), whereas the shape of the $^{[6]}$Al peak at 9.4 T might suggest two sites with different $C_q$ and $\delta_{iso}$ values. The 9.4-T $^{27}$Al 3QMAS NMR spectrum of natural kaolinite (Figure 12 C) again demonstrates the presence of only one site, whereas that of CAW1964 (Figure 12 D) at 14.1 T suggests multiple but unresolved $^{[6]}$Al sites with similar atomic environments and thus similar $\delta_{iso}$ and $C_q$ values.

## Conclusions

$^{17}$O and $^{27}$Al MAS and MQMAS at high fields provide much improved spectral resolution for the oxygen and aluminum sites of layer silicates than previous MAS NMR studies and allow discrimination of crystallographically distinct basal, apical, and hydroxyl sites. These oxygen sites have well-defined ranges of $C_q$ and isotropic chemical shift (Figure 9). Further studies with phase-pure samples might allow peak assignment for the basal oxygen sites. Detailed SSB manifold analysis yields precise values of $^{27}$Al NMR parameters that cannot be obtained from $^{27}$Al 3QMAS NMR data or $^{27}$Al MAS data alone. Good quantification of the $^{[6]}$Al/$^{[4]}$Al ratio is achieved in $^{27}$Al MAS NMR spectroscopy at high field.

**Acknowledgment.** This project was supported by a Stanford Graduate Fellowship and a Carnegie Postdoctoral Fellowship to S.K.L., NSF Grant EAR 01004926 to J.F.S., and NSF Grant EAR90-04260 to R.J.K.. We thank R. Jones for help with SEM analysis. We also thank Dr. P. Zhao for pulse sequence development. We are grateful to Professor J. Puglisi for access to, and Drs. L. Du and C. Liu for assistance with, the 18.8-T spectrometer in the Stanford Magnetic Resonance Laboratory. We also thank Dr. Z. Xu, Dr. H. Eckert, and three anonymous reviewers for helpful comments.

CM030165H

(50) Ashbrook, S. E.; Berry, A. J.; Wimperis, S. *J. Phys. Chem. B.* **2002**, *106*, 773−778.

(51) Rocha, J. *J. Phys. Chem. B.* **1999**, *103*, 9801−9803.